

## Induced airflow in flying insects

### I. A theoretical model of the induced flow

Sanjay P. Sane

*Department of Biology, University of Washington, Seattle, WA 98195, USA*

e-mail: sane@u.washington.edu

*Accepted 21 October 2005*

#### Summary

**A strong induced flow structure envelops the body of insects and birds during flight. This flow influences many physiological processes including delivery of odor and mechanical stimuli to the sensory organs, as well as mass flow processes including heat loss and gas exchange in flying animals. With recent advances in near-field aerodynamics of insect and bird flight, it is now possible to determine how wing kinematics affects induced flow over their body. In this paper, I develop a theoretical model based in rotor theory to estimate the mean induced flow over the body of flapping insects. This model is able to capture some key characteristics of mean induced flow over the body of a flying insect. Specifically, it predicts that induced flow is directly proportional to wing beat frequency and stroke amplitude and is also affected by a**

**wing shape dependent parameter. The derivation of induced flow includes the determination of spanwise variation of circulation on flapping wings. These predictions are tested against the available data on the spanwise distribution of aerodynamic circulation along finite *Drosophila melanogaster* wings and mean flows over the body of *Manduca sexta*. To explicitly account for tip losses in finite wings, a formula previously proposed by Prandtl for a finite blade propeller system is tentatively included. Thus, the model described in this paper allows us to estimate how far-field flows are influenced by near-field events in flapping flight.**

Key words: spanwise circulation, self-generated flow, rotor theory, tip loss, near-field flow, far-field flow.

#### Introduction

Flapping birds and insects are often likened to revolving propeller blades or rotors because their wings generate lift by steadily pushing air downward. Two influential aerodynamic models of flight in insects (Ellington, 1984c) and birds (Rayner, 1979) drew much inspiration from the extensive theoretical work on rotor aerodynamics. These models focused primarily on the far-field wake of flapping wings using the conceptual abstraction of a pulsed actuator disk, albeit with appropriate modifications to account for the changes in stroke angles and other correction factors appropriate for birds or insects (Rayner, 1979; Ellington, 1984c). Although successful in capturing some interesting far-field features due to flapping wings (e.g. vortex gaits) and stroke-averaged parameters such as power, efficiency etc., subsequent researchers were unable to synthesize these far-field theories with near-field aerodynamics of flapping wings, primarily due to a lack of understanding of the major components of aerodynamic force generation in high-angle of attack flapping flight.

In the last decade, several groups focused their attention on detailed aerodynamic measurements (Dickinson et al., 1999; Sane and Dickinson, 2001; Usherwood and Ellington, 2002; Dickson and Dickinson, 2004; Maybury and Lehmann, 2004)

and flow visualization on scaled flappers (VandenBerg and Ellington, 1997b; Birch and Dickinson, 2001) and flapping insects (Dickinson and Gotz, 1996; Willmott et al., 1997; Srygley and Thomas, 2001; Bomphrey et al., 2005). In addition to these experiments, there are also several new Computational Fluid Dynamic (or CFD) simulations of flow around flapping insect wings (Liu et al., 1998; Ramamurti and Sandberg, 2002; Sun and Tang, 2002; Wang et al., 2004; Miller and Peskin, 2005) and a few analytic models (Minotti, 2002; Zbikowski, 2002). Together, these researches have vastly improved our understanding of the near-field mechanisms of force production by flapping wings. However, unlike earlier descriptions of wakes behind insects and birds, these studies focused almost exclusively on the proximate mechanisms of aerodynamic force generation (for reviews, see Sane, 2003; Wang, 2005).

Due to these advances on the experimental and numerical front, it is now possible to address how far-field flow is related to near-field aerodynamic mechanisms. In addition, because the flow environment greatly influences many biological processes such as olfaction or mass flow, such calculations may be especially useful to researchers who work on the interface of flight and sensory-motor physiology. For instance,

a detailed understanding of induced flow can allow us to determine the odor plume dynamics over the antennae during flight and understand how moths and other insects accurately track odors. It may also be important from the physiological perspective to understand, for instance, how convective heat loss is enhanced by induced flow, thus influencing the overall flight energetics in endothermic insects.

The main aim of this two-part paper is to estimate the magnitude of the gross flows around an insect body using the near-field approach and discuss their biological importance. The first part of this study presents a derivation of induced airflow using helicopter (or rotor) theory and a blade element-momentum approach modified for application to hovering insects. This model is used to predict the magnitude of mean self-generated air flow in flying insects. In the second paper (Sane and Jacobson, 2006), we test some of the theoretical predictions *via* systematic measurements of the magnitude of self-generated airflow along the insect body using hot-wire anemometry and show that in addition to the mean induced flow predicted by the theory outlined here, there are additional higher frequency components due to flapping wing motion. We will discuss the relevance of these mean flows and higher frequency flow fluctuations to animal flight studies.

## Materials and methods

### Induced velocity model

#### Overview and main assumptions

Many recent studies show that at Reynolds number over *ca.* 100, the flows and forces due to flapping wings are well approximated by Euler equations (Wang, 2000; Ramamurti and Sandberg, 2002; Sane and Dickinson, 2002; Sun and Tang, 2002). Therefore, the model presented in this paper assumes the fluid to be essentially inviscid and incompressible. The effects of vortices, which have their origins in viscous interactions at solid–fluid boundaries, are incorporated into the model through use of empirical coefficients. For example, the influence of leading edge vorticity and tip vorticity is implicitly included within the main derivation of circulation through the use of lift coefficients measured on the finite wings. Although this procedure considerably simplifies the model in the initial stages, there is evidence from both propeller (Leishman, 2000) and insect flight literature (Birch et al., 2004) that tip losses contribute directly and significantly to the overall flow structure. Several approximate empirical formulae have been previously proposed but none offer exact solutions to account for tip losses. The earliest of these formulations, developed by Prandtl (for reviews, see Johnson, 1980; Seddon, 1990; Leishman, 2000; see also Jones, 1990 for a review on finite wing theory) for a two dimensional (2D) far-wake resulting from a finite number of rotor blades, modeled the effect of tip loss in terms of a decrease in the effective actuator disk radius. It predicted a reduction in effective blade radius as the number of blades in the propeller system decreased. As the number of blades tends to infinity, the propeller blades

approximate an actuator disk and the effect of tip losses is minimal. Given the sparse data on sectional lift characteristics of flapping insect wings, Prandtl's approach is arguably the simplest to incorporate within a blade-element model and will be tentatively incorporated in the theory described here (see Discussion). Finally, because the current model is based on rigid propeller theory, the aerodynamic effects of wing rotation at either end of the stroke (Dickinson, 1994; Dickinson et al., 1999; Sane and Dickinson, 2002) are ignored but can be incorporated in future extensions of this model.

#### Calculation of self-generated airflow

For a rigid wing of length  $R$  flapping about an axis with an angle of attack  $\alpha(t)$  and an angular velocity  $\dot{\phi}$ , the velocity of the wing at any span-wise location  $r$  is given by:

$$u_{\infty}(r) = \dot{\phi} r. \quad (1)$$

Because a wing flapping with a frequency of  $n$  and stroke amplitude of  $\Phi$  travels through a total angle of  $2\Phi$  every  $1/n$  s, the mean wing speed at any point at a distance  $r$  from the base is:

$$u_{\infty}(r) = 2\Phi nr. \quad (2)$$

The wing may now be divided into several blade elements such that each blade element is located at a distance  $r$  from the base and is of width  $dr$  and chord length  $c(r)$ . From the Biot–Savart's law, we can calculate the induced flow at any point in the vicinity of wing by integrating the ratio of spanwise changes in the sectional circulation to the distance of the blade element from the point of interest, over the entire span of a flapping wing (Prandtl and Tietjens, 1957; Milne-Thomson, 1973). Thus, if the circulation around each such blade element is  $\Gamma(r)$  then the flow speed  $v_i$  induced by this element at a point P located at a distance  $x$  from the base (Fig. 1A) is given by:

$$v_i(x) = -\frac{1}{4\pi} \int_0^R \frac{d\Gamma}{dr} \frac{dr}{x-r}. \quad (3)$$

For an inclined flapping wing,  $\Gamma(r)$  includes the circulation due to the leading edge vortex. In the domain  $0 < x < R$  there exists at least one point  $x=r$ , where the integral in Eqn 3 is improper, with a Cauchy-type kernel that tends to infinity. However, because a vortex cannot induce velocity at its own core, for all points on the wing ( $0 < x < R$ ), we can eliminate the point  $x=r$  and convert the improper integral to a non-singular form. This allows us to take the principal value of the integral using the equation:

$$v_i(x) = -\frac{1}{4\pi} \lim_{\epsilon \rightarrow 0} \left\{ \int_0^{x-\epsilon} \frac{\left(\frac{d\Gamma}{dr} dr\right)}{(x-r)} + \int_{x+\epsilon}^R \frac{\left(\frac{d\Gamma}{dr} dr\right)}{(x-r)} \right\}, \quad (4)$$

where  $\epsilon$  is infinitesimally small. This method allows the integral in Eqn 4 to attain a convergent form whose value

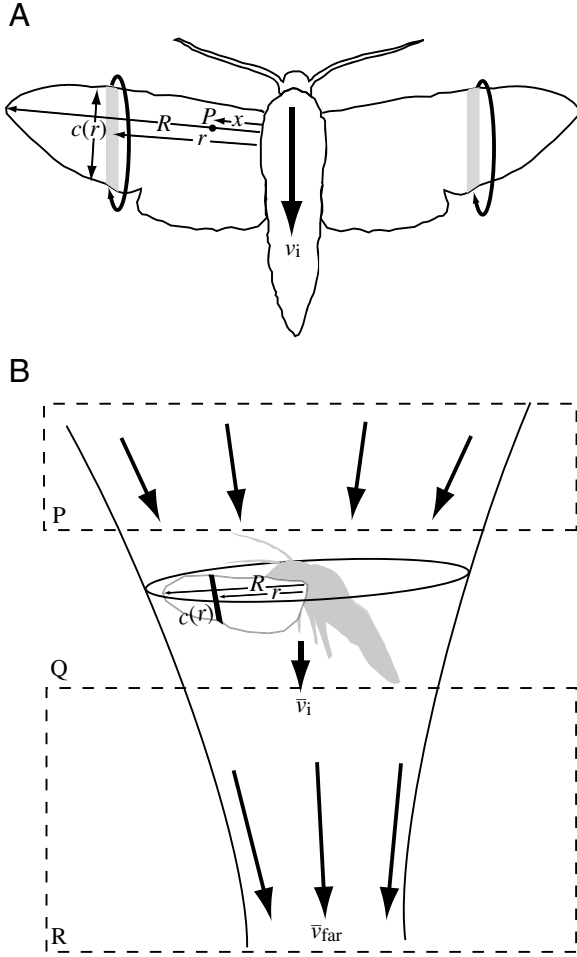


Fig. 1. The Induced Flow Model. (A) Blade element model. A schematic of the flapping wings of an insect. The grey strips show one of the elements of the blade element model, with the sectional circulation around it. (B) Momentum Flux Model. Extension of the near-field model in A to the far-field. The regions around the flying insect are divided into far-field inflow (P), near-field (Q), and far-field outflow (R). In this figure,  $\bar{v}_i$  and  $\bar{v}_{far}$  represent the near-field outflow and far-field outflow based on standard actuator disk theory.

depends on how  $\Gamma$  varies with  $r$  (e.g. Prandtl and Tietjens, 1957; Milne-Thomson, 1973, p. 80).

#### Determination of a circulation profile along the wing span

The functional form of  $\Gamma(r)$  may be determined using a semi-empirical approach in which the value of the net circulation around the wing is calculated using measured aerodynamic force coefficients. In addition, the model assumes that the quasi-steady condition holds and the aerodynamic coefficients are time independent. Thus, the induced velocity depends only on the instantaneous spatial distribution of circulation on each flapping wing. From these considerations, the lift per unit span is given by:

$$\frac{dF_L}{dr} = \frac{1}{2} \rho C_L(r) u_\infty^2(r) c(r). \quad (5)$$

From standard Kutta–Jukowski theory, the lift per unit span around a 2D wing or any section of an infinite wing is given in terms of circulation by:

$$\frac{dF_L}{dr} = \rho u_\infty(r) \Gamma_{2D}(r), \quad (6)$$

where the subscript 2D refers to the condition that circulation around every section on the wing is assumed to be equal to the circulation around a 2D wing translating with a velocity  $u_\infty(r)$ . Here, the  $r$  dependence in the expression for  $\Gamma_{2D}(r)$  arises from the differential translational velocity of each wing section. This is shown by equating Eqn 5 and 6 and rearranging terms to obtain the circulation around a wing section in terms of lift coefficient, wing geometry and wing velocity,

$$\Gamma_{2D}(r) = \frac{1}{2} C_L(r) u_\infty(r) c(r), \quad (7)$$

and substituting Eqn 2 in Eqn 7:

$$\Gamma_{2D}(r) = C_L(r) \Phi n r c(r). \quad (8)$$

Using the conventional scheme outlined by Ellington (1984a,b), we can non-dimensionalize  $r$  with respect to wing length  $R$  and divide  $c(r)$  by the mean chord  $\bar{c}$ . Eqn 8 can thus be rewritten as:

$$\hat{r} = \frac{r}{R}, \quad (9a)$$

$$\hat{c}(\hat{r}) = \frac{c(\hat{r})}{\bar{c}}, \quad (9b)$$

$$\Gamma_{2D}(\hat{r}) = \Phi n R \bar{c} C_L(\hat{r}) \hat{r} \hat{c}(\hat{r}). \quad (9c)$$

Extending this equation to the finite wing case imposes certain physical constraints on  $\Gamma_{2D}(\hat{r})$ . For a fixed wing of finite span, the tip of the wing generates zero lift whereas the lift is maximum at the base of each wing (or the center of the two wing system). Thus, the circulation at the wing base corresponds to maximum lift and falls elliptically from base to tip. This condition is typically incorporated using the method of Betz as follows:

$$\Gamma_f(\hat{r}) = \sqrt{1 - \hat{r}^2} (\Gamma_0 + \Gamma_2 \hat{r}^2 + \Gamma_4 \hat{r}^4 + \dots), \quad (10)$$

where  $\Gamma_0$  corresponds to the maximum value of the section situated at the center of the fixed wing system (or the base of each wing) and  $\Gamma_2, \Gamma_4, \dots$  are second, fourth etc. derivatives of the circulation with respect to  $\hat{r}$  (Milne-Thomson, 1973) and the subscript  $f$  refers to a wing of finite span. To a first approximation, with smoothly varying  $\Gamma_f$  and  $0 \leq \hat{r} \leq 1$ , this formula is typically written as:

$$\Gamma_f(\hat{r}) = \Gamma_0 \sqrt{1 - \hat{r}^2}. \quad (11a)$$

The subscript  $f$  refers to a finite wing (Prandtl and Tietjens,

1957; Kuethe and Chow, 1986). For the case of finite revolving wings,  $\Gamma_0$  is simply the circulation of a given wing section varying with  $\hat{r}$ . The semi-elliptic distribution is thus further modified by the linear variation in velocity from the base to the tip of the wing. Physically, this is incorporated by equating:

$$\Gamma_0 = \Gamma_{2D}(\hat{r}). \quad (11b)$$

The net distribution of  $\Gamma_r(\hat{r})$  along the span of a rotating rectangular finite propeller blade is thus a combination of linear and elliptic distributions.

Except at the end of each stroke, the motion of an insect wing blade can be modeled as a rotating propeller blade. Thus, by incorporating the measured coefficients of aerodynamic forces from the extensive experimental data on mechanical models of flapping wings (for a review, see Sane, 2003), we can extend the conclusions of the propeller theory to insect flight. Further assuming that the general features of the circulation distribution on a rotating propeller blade also hold true for flapping insect wings, it is possible to extend them to the far-field flow using standard propeller theory. Combining Eqn 8 and Eqn 11a,b yields:

$$\Gamma_r(\hat{r}) = \Phi n R \bar{c} C_L(\hat{r}) \hat{r} \hat{c}(\hat{r}) \sqrt{1 - \hat{r}^2}. \quad (12)$$

Here, to accommodate the quasi-steady assumption, we assume that  $C_L(\hat{r})$  is the steady lift coefficient, i.e. it varies only spatially along the wing span but does not explicitly depend on time or flow history.

#### Spanwise variation in lift coefficient

For infinite wings or wings with high aspect ratio, the distribution of lift coefficient is usually assumed to be constant along the entire length of the wing. For flat or twisted finite rotor blades or low aspect ratio wings however, the lift coefficients may be substantially modified by a local variations in sectional inflow leading to a spanwise variation in effective angles of attack from base to tip (Birch and Dickinson, 2001; Usherwood and Ellington, 2002). For flapping insect wings, we must also include further modifications due to the geometry of the wing and twist on local angles of incidence.

Although the effects of wing velocity gradient and geometry can be determined using flapping kinematics and wing morphology, respectively, we must rely on empirical measurements to determine the spanwise variation in lift coefficient. Previous models of lift distribution have generally assumed aerodynamic force coefficients to be constant over the entire length of the span (e.g. Ellington, 1974). Recent measurements on a wide variety of wing shapes also reveal that although the gross force coefficients do not vary greatly as a function of wing geometry (Usherwood and Ellington, 2002; Wang et al., 2004), there is a substantial change in sectional angles of attack from base to tip, which causes a corresponding change in sectional lift coefficients. In revolving wings, force measurements as well

as particle image flow visualization on flapping model wings (Birch and Dickinson, 2001) show that the sectional angles of attack increase monotonically from base to tip. This effect may further combine with a spanwise increase in the size of the leading edge vortex (Ellington et al., 1996; VandenBerg and Ellington, 1997a; Birch et al., 2004). Based on numerical simulations showing that the coefficient of lift varies as a slow rising function of radial position with a zero intercept for an untwisted propeller blade (Leishman, 2000, p. 95), the sectional lift coefficient is modeled here as a linear function of spanwise position to a first approximation:

$$C_L(\hat{r}) = K_0 \hat{r}, \quad (13)$$

where  $K_0$  is a proportionality constant.

Because experiments on mechanical flappers typically measure the force coefficients after the initial transients have subsided and a steady induced flow has been established, the mean lift coefficient  $\bar{C}_L$  depends not on the angle of attack relative to the free stream at the onset of flapping, but also relative to an entrained free stream several strokes later (Birch and Dickinson, 2001; Usherwood and Ellington, 2002; Birch and Dickinson, 2003). Also, these experiments typically measure forces at the base of the wing, thus yielding the average post-transient lift coefficients  $\bar{C}_L$  due to an integrated sum of instantaneous sectional circulations along the span. Thus,

$$\bar{C}_L = \frac{\int_0^1 C_L(\hat{r}) d\hat{r}}{\int_0^1 d\hat{r}}. \quad (14)$$

Substituting  $C_L(\hat{r})$  from Eqn 13 and solving for  $K_0$ , we get:

$$C_L(\hat{r}) = 2\bar{C}_L \hat{r}. \quad (15)$$

This expression when substituted in Eqn 12 gives:

$$\Gamma_r(\hat{r}) = 2\bar{C}_L \Phi n R \bar{c} \hat{r}^2 \hat{c}(\hat{r}) \sqrt{1 - \hat{r}^2}. \quad (16)$$

Alternatively, we can express  $\Gamma_r(\hat{r})$  in terms of tip velocity of the wing as:

$$\Gamma_r(\hat{r}) = \bar{C}_L u_\infty(R) \bar{c} \left[ \hat{r}^2 \sqrt{1 - \hat{r}^2} \hat{c}(\hat{r}) \right]. \quad (17)$$

Substituting  $\Gamma_r(\hat{r})$  from Eqn 16 in Eqn 3 in dimensionless form gives an expression for induced velocity for a wing of any planform:

$$v_i(\hat{x}) = - \frac{\bar{C}_L \Phi n \bar{c}}{2\pi} \int_0^1 \frac{\left[ \frac{d \left[ \hat{r}^2 \sqrt{1 - \hat{r}^2} \hat{c}(\hat{r}) \right]}{d\hat{r}} \right]}{\hat{x} - \hat{r}} d\hat{r}, \quad (18)$$

where  $\hat{x}$  is any arbitrary point on or near the moving wing.

### Sectional variation in chord length

Eqn 18 provides a general form for induced flow without specifying its explicit dependence on wing geometry. Because there is considerable interspecific variation in wing geometry in various insects, it is useful to develop a procedure for estimating non-dimensional chord length  $\hat{c}(\hat{r})$ , which can be used to derive analytical estimates of induced flow speeds. This is possible with an appropriate choice of  $\hat{c}(\hat{r})$  that not only describes the wing shape, but also allows us to avoid the singularity at 1 or 0.

In his analysis of insect wing morphology, Ellington (1984a) noted that for many insect wings,  $\hat{c}(\hat{r})$  is accurately described using a standard Beta distribution, which is only defined in the domain [0, 1]. He noted that, for any given wing, there usually exists a Beta function describing spanwise variation of chord length. In this analysis, I adopt Ellington's method and represent  $\hat{c}(\hat{r})$  using Beta functions appropriately rescaled with a constant non-dimensional parameter  $B_i$ , the ratio of maximum non-dimensional chord length for actual insect wing ( $\hat{c}_{\text{insect,max}}$ ) to the maximum non-dimensional chord length for the Beta function ( $\hat{c}_{\text{max}}$ ). Thus,

$$B_i = \frac{\hat{c}_{\text{insect,max}}}{\hat{c}_{\text{max}}}, \quad (19a)$$

$$\hat{c}(\hat{r}) = \hat{r}^p(1-\hat{r})^q, \quad (19b)$$

where  $p, q > 0$  for all cases and  $q > 0.5$  for most insect wings. Substituting Eqn 19a,b in Eqn 16 and multiplying the right hand side by  $B_i$  yields the dimensional circulation:

$$\Gamma_f(\hat{r}) = 2\Phi n R \bar{C}_L \bar{c} B_i [\hat{r}^{p+2}(1-\hat{r})^{q+\frac{1}{2}}(1+\hat{r})^{\frac{1}{2}}]. \quad (20)$$

Eqn 20 provides the most general relationship for the distribution of circulation on a single flapping wing. Differentiating,

$$\frac{d\Gamma_f(\hat{r})}{d\hat{r}} = 2\Phi n \bar{C}_L \bar{c} B_i \hat{r}^{p+2}(1-\hat{r})^{q+\frac{1}{2}}(1+\hat{r})^{\frac{1}{2}} \left\{ \frac{p+2}{\hat{r}} - \frac{2q+1}{2(1-\hat{r})} + \frac{1}{2(1+\hat{r})} \right\}. \quad (21)$$

Substituting in Eqn 3, we get:

$$v_i(\hat{x}) = \frac{\Phi n \bar{C}_L \bar{c} B_i}{2\pi} \int_0^1 \frac{\hat{r}^{p+2}(1-\hat{r})^{q+\frac{1}{2}}(1+\hat{r})^{\frac{1}{2}} \left\{ \frac{p+2}{\hat{r}} - \frac{2q+1}{2(1-\hat{r})} + \frac{1}{2(1+\hat{r})} \right\} d\hat{r}}{\hat{r} - \hat{x}}. \quad (22)$$

Eqn 22 provides a general relationship induced velocity due to a single flapping wing at a point located at distance  $\hat{x}$  from the base of the wing. The contribution from the second wing must be added to this with the appropriate modified value of  $\hat{x}$  with

reference to the other wing. Because  $p > 0$  and  $q \geq 0.5$  for most insect wings, the integral in Eqn 22 takes on finite values for all values of  $\hat{x} < 0$  and  $\hat{x} > 1$ , but in the domain of  $\hat{r}$  ( $1 < \hat{x} < 0$ ), this integral must be converted to a principal value integral and solved as shown by Eqn 4.

Below, I will describe how Eqn 22 applies to *Drosophila* and *Manduca*, for which there is some experimental data on induced flow. To measure the values of  $c(r)$ , the outlines of a *Drosophila* wing and a *Manduca* wing were traced on to a graph paper and divided respectively into 28 and 50 strips of equal thickness. The length of each strip  $c(r)$  was plotted against the position  $r$  of that strip with respect to the base (Fig. 2A,B, filled circles) for a wing of normalized length. The resulting plot depicts how  $c(r)$  varies as a function of the non-dimensional position ( $r$ ).

The parameters in Eqn 19 approximate a *Drosophila* wing for  $p=0.75$ ,  $q=0.5$  and  $B_{\text{fly}}=3.2$  (Fig. 2A) and a *Manduca* wing for  $p=0.125$ ,  $q=0.5$  and  $B_{\text{moth}}=1.8$  (Fig. 2B). For any given value of  $\hat{x}$ , the integrand in Eqn 22 depends only on the morphology of the wing and thus may be denoted by an induced velocity shape factor denoted by  $s_i$ , where:

$$s_i(\hat{x}) = \int_0^1 \frac{\hat{r}^{p+2}(1-\hat{r})^{q+\frac{1}{2}}(1+\hat{r})^{\frac{1}{2}}}{\hat{r} - \hat{x}} \left\{ \frac{p+2}{\hat{r}} + \frac{1}{2(1+\hat{r})} - \frac{1+2q}{2(1-\hat{r})} \right\} d\hat{r}. \quad (23)$$

Along the length of the wing, this integral is difficult to solve analytically because it has a Cauchy-type kernel that goes to infinity for  $\hat{x}=\hat{r}$ . A method to solve such integrals is outlined by Prandtl in a paper by Betz (Milne-Thomson, 1973), but not without making the derivations tedious and the conclusions difficult to apply generally.

Because the trailing edge vorticity is shed into the region behind the stroke plane, there is greater unsteadiness of the flow in the outflow regions than in the inflow regions where the fluid entrainment is influenced primarily by the bound vorticity of the flapping wings. The starting and stopping vortices, while certainly existing within the flow field, have a very limited effect on the axial inflow because they are rapidly convected downstream by a unidirectional induced flow field. Along the axis in the outflow regions, the effect of starting and stopping vortices is further mitigated by the mutual annihilation of the opposing vorticity of the two wings (Lehmann et al., 2005). For these reasons, to keep the model simple and easily testable, I focus on the simplest case of axial inflow ( $\hat{x}=0$ ) where the effects of starting and stopping vortices is minimal. Substituting Eqn 23 in Eqn 22 gives:

$$v_i(\hat{x}) = \left( \frac{\bar{C}_L \Phi n \bar{c} B_i}{2\pi} \right) s_i(\hat{x}). \quad (24)$$

At the base  $\hat{x}=0$  and the induced velocity due to each wing is given by:

$$v_i(0) = \left( \frac{\bar{C}_L \Phi n \bar{c} B_i}{2\pi} \right) s_i(0), \quad (25)$$

where  $s_i(0)$ , the induced velocity shape factor evaluated at the base is given by:

$$s_i(0) = \int_0^1 \hat{r}^{p+1} (1-\hat{r})^{q+\frac{1}{2}} (1+\hat{r})^{\frac{1}{2}} \left\{ \frac{p+2}{\hat{r}} + \frac{1}{2(1+\hat{r})} - \frac{1+2q}{2(1-\hat{r})} \right\} d\hat{r}. \quad (26)$$

The integral  $s_i(0)$  is easily solvable for  $p > 0$  and  $q \geq 0.5$ . For most, if not all cases, the values of  $p$ ,  $q$  for wings obey these values. We can now use Eqn 25 to determine the induced velocity at the base of the wing. Because the flow at the center of the two wing system is axi-symmetric, the axial inflow velocity at the base of the wing ( $\hat{x}=0$ ) is simply twice the value for each wing and is given by:

$$v_{\text{axial}} = \left( \frac{\bar{C}_L \Phi n \bar{c} B_i}{\pi} \right) s_i(0). \quad (27)$$

Eqn 27 offers some simple and testable predictions for induced axial flow along the body of the insect. First, for constant stroke amplitude, the induced axial velocity is directly proportional to wing beat frequency. Second, for constant wing beat frequency, induced axial velocity is directly proportional to stroke amplitude. Third, if both stroke amplitude and wing beat frequency are variable, these two predictions can be combined to obtain a more general prediction that the induced axial velocity is directly proportional to the wing velocity.

#### Effective angle of attack

A spanwise variation in downwash leads to corresponding variation in sectional angles of attack. To determine this variation, we can derive the sectional angle of attack from the ratio of sectional induced flow velocity to the wing velocity at a spanwise station on the wing located at a distance  $\hat{x}$  from the base. Assuming that the effect of the image wing is negligible, we can divide the induced flow at any section by the local wing velocity given by Eqn 2 to obtain:

$$\frac{v_i(\hat{x})}{u_\infty(\hat{x})} = \frac{\bar{C}_L \bar{c} B_i}{4\pi R} \left( \frac{s_i(\hat{x})}{\hat{x}} \right). \quad (28)$$

Substituting the aspect ratio  $\mathcal{AR} = 2R/\bar{c}$ , we get:

$$\frac{v_i(\hat{x})}{u_\infty(\hat{x})} = \frac{\bar{C}_L}{\pi \mathcal{AR}} \left( \frac{B_i s_i(\hat{x})}{2\hat{x}} \right). \quad (29)$$

This result can be readily compared with the standard result for fixed airfoils  $v_i/u_\infty = \bar{C}_L/\pi \mathcal{AR}$ . In case of a flapping wing, the ratio of sectional induced velocity to sectional velocity is also dependent on the span wise position by a factor  $[B_i s_i(\hat{x})]/2\hat{x}$ . The effective angle of attack at any spanwise position  $\hat{x}$  is thus given by:

$$\alpha'(\hat{x}) = \alpha - \tan^{-1} \left( \frac{v_i(\hat{x})}{u_\infty(\hat{x})} \right), \quad (30)$$

where  $\alpha'(\hat{x})$  is the sectional angle of attack and  $\alpha$  is the morphological angle of attack.

#### Flow velocities in the far wake

Because the flapping wing is the only source of vorticity generation in the field, we may treat the rest of the fluid outside this region as irrotational. Assuming the fluid to be inviscid and incompressible, we can apply the Bernoulli theorem for the flow within these regions. Thus, the main results of the classical models based on standard actuator disk theory should hold in the non-vortical regions A and B (Fig. 1).

The standard actuator disk theory is based on the assumption that a rotor (or propeller) may be approximated by a 2D disk, which generates uniform and steady pressure difference above and below the disk, thereby generating sufficient forces for weight offset during hovering. This theory, when applied to insect (Ellington, 1984c) and bird flight (Rayner, 1979), retained the assumption of radial uniformity of pressure distribution but replaced the steady pressure difference with pressure pulses generated over each stroke. Although the theory outlined in previous sections depends on the radial increase in velocity for a rotating propeller blade or wing, such non-uniformity is smeared out in the far field due to the presence of the slightest viscosity in actual fluids. Hence, when extending the near field theory to far-field, it is convenient to retain most assumptions of the actuator disk theory. The section below repeats some of the theory from previous publications (Rayner, 1979; Ellington, 1984c) but is included here for the sake of completeness.

If the mean induced velocity averaged over the entire disk surface is  $\bar{v}_i$  and mean pressure is  $P$ , the total head at the disk is  $P + 1/2(\rho \bar{v}_i^2)$ . With an ambient pressure  $P_0$ , and far-field velocity below the disk,  $\bar{v}_{\text{far}}$ , because  $P_0 > P$ , there is a continuous flow of air along the length of the insect body of mass  $m$  throughout the duration of flapping. Bernoulli's theorem equates the difference in total pressure head at the disk to the net momentum flux: Above the disk,

$$P_0 = P + \frac{1}{2} \rho \bar{v}_i^2, \quad (31)$$

and below the disk,

$$P + \frac{mg}{A} + \frac{1}{2} \rho \bar{v}_i^2 = P_0 + \frac{1}{2} \rho \bar{v}_{\text{far}}^2. \quad (32)$$

Thus,

$$\bar{v}_{\text{far}} = \sqrt{\frac{2mg}{\rho A}}, \quad (33)$$

$$\int_0^R dF_L = \frac{d}{dt} (m \bar{v}_i). \quad (34)$$

Thus, because left hand side equals the animal's weight and right hand side equals the net momentum flux,

$$mg = \rho \bar{v}_i \bar{v}_{\text{far}} A. \quad (35)$$

Rearranging,

$$\bar{v}_{\text{far}} \bar{v}_i = \frac{mg}{A\rho}. \quad (36)$$

Thus, from Eqn 33 and 36, we get the standard result:

$$\bar{v}_{\text{far}} = 2\bar{v}_i. \quad (37)$$

Because of the assumption of continuity, the cross-sectional area of the disk (or stream tube) changes inversely as the velocity. Thus, if the area of the actuator disk is  $A$ , the cross-sectional area of the tube in the far-field  $A_{\text{far}}$  is:

$$A_{\text{far}} = \frac{A}{2}. \quad (38)$$

Because of the complexities introduced by the presence of image wings, the relationship between far field flow and near field flow is best determined for the case of the axial velocities. Thus at the core of the flow, substituting from Eqn 27:

$$v_{\text{far}}(0) = \frac{2\bar{C}_L \Phi n \bar{c} B_i}{\pi} s_i(0). \quad (39)$$

Because the flows are eventually dissipated by viscosity in the case of real fluids, the region of applicability for the formula given by Eqn 39 is somewhat limited.

## Results and discussion

To illustrate how this theory can be applied to experimental data, this section will focus on data from *Drosophila* and *Manduca*, two of the best studied examples for insect flight. These examples also offer us data for a rigorous test of the theory because of the different sizes of these insects as well as their different wing planforms. For each example, I will focus only on those predictions for which experimental data is available.

### Sectional circulation along the wing span

#### Case study: *Drosophila melanogaster*

Recent calculations of circulation derived from Digital Particle Image Velocimetric (DPIV) measurements of the flow around wing sections for model *Drosophila* wings (Birch et al., 2004) provide a direct experimental data to test the model for induced flow.

As described in Fig. 2A, the form of  $\hat{c}(\hat{r})$  for a *Drosophila* wing is approximated quite well by the Eqn 19:

$$\hat{c}(\hat{r}) = \hat{r}^{0.75}(1-\hat{r})^{0.5}. \quad (40)$$

Using  $p=0.75$ ,  $q=0.5$  and  $B_{\text{fly}}=3.2$ , Eqn 20 allows us to calculate chord as a function of wing position. Using Eqn 20

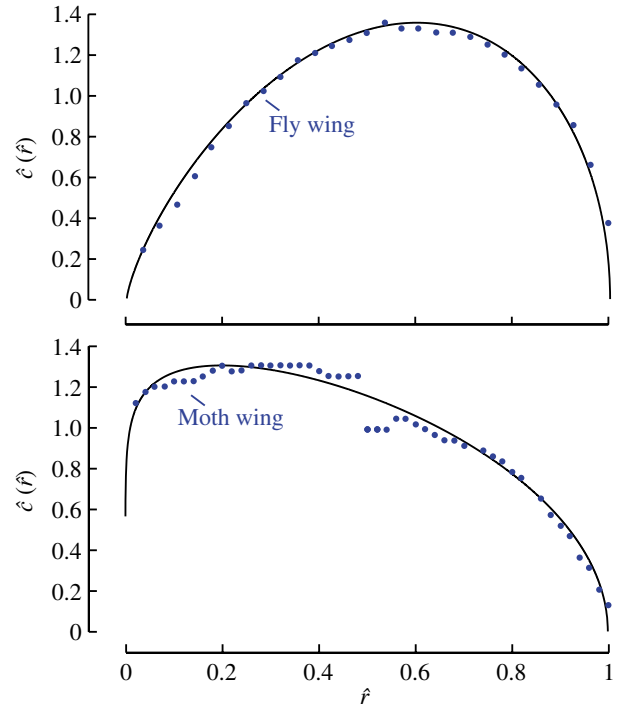


Fig. 2. Beta function fits to wing morphology. Filled blue circles show actual data points measured for  $\hat{c}(\hat{r})$  in (A) *Drosophila melanogaster* (fly) wing and (B) *Manduca sexta* (moth) wing. The black curves are Beta functions generated by the Eqn 40 for *Drosophila melanogaster* (A) and Eqn 46 for *Manduca sexta* wing (B).

in the current model, I estimated the spanwise circulation as a function of non-dimensionalized distance from the base. This estimate is derived from the assumptions of quasi-steady state and a semi-elliptical distribution of forces along the wing span. The normalized functional forms of  $\hat{c}(\hat{r})$ ,  $\hat{r}^2\sqrt{1-\hat{r}^2}$  and  $\Gamma_{\text{f}}(\hat{r})$  are given in Fig. 3A.

A similar approach for deriving spanwise circulation was proposed tentatively by Ellington (1974), who also suggested a linearly varying component of the circulation arising from spanwise changes in velocity. However, the nearly-elliptic component in Ellington (1974) arises from a variation in chord as a function of span wise position,  $c(r)$ . In contrast, in the above described framework, the nearly elliptic variation arises from a combination of  $c(r)$  and a quasi-steady elliptic distribution of circulation on any finite airfoil. Thus, the essential form of the function – its slow rise to a maximum value followed by a roll-off towards the tip – would hold even for a finite rectangular wing. This is true, for instance, in a rectangular helicopter blade (Conlisk, 1997).

Fig. 3B shows a comparison of the circulation calculated using the above model and the circulation measured from sectional flow vector fields in (Birch et al., 2004). The measurements of circulation were performed on a model *Drosophila* wing flapping in a tank of oil filled with air bubbles as seeding particles and systematically imaging the flow fields around each span wise section using Particle Image Velocimetry (Birch et al., 2004). The functional form of

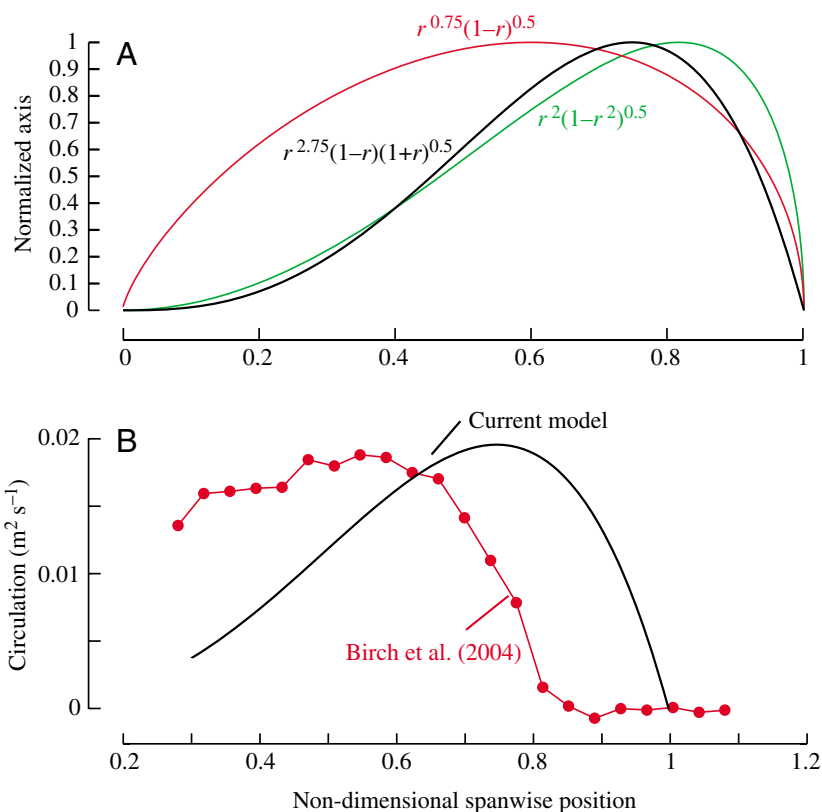


Fig. 3. Circulation along the wing span. (A) Circulation as a function of non-dimensional spanwise position for the case example of a *Drosophila* wing. The red curve shows the functional form of chord length as a function of non-dimensional spanwise position, and the green curve shows the functional form of circulation for a revolving propeller blade with a varying lift coefficient that varies linearly from base to tip. The black curve depicts the final functional form of the circulation on an insect wing obtained by multiplying the values generating the red and blue curves. (B). Comparison of the theoretically derived circulation variation with an experimentally derived distribution of circulation from DPIV data in a model *Drosophila* wing from Birch et al. (2004).

circulation in the model is constructed from physical considerations and scaled using force coefficients, kinematic parameters and wing morphology, whereas the measurement and subsequent estimation of circulation were carried out without *a priori* knowledge of the forces or force coefficients or any assumptions about the nature of spanwise variation. Thus, in principle, these two estimates are entirely independent. Hence, the similarity in measured and predicted magnitudes validates this model. The location of the peak of  $\Gamma$  in real wings should not necessarily match the theoretical model that neglects tip loss.

Using the values of tip velocity from Birch et al. (2004) of  $0.26 \text{ m s}^{-1}$ , mean chord ( $\bar{c}$ ) of 7 cm, and lift coefficient of 1.8 and the analytic function for the wing shape of a fly described above, the spanwise circulation as a function of non-dimensional distance from the base is shown in Fig. 3B. The results of these two estimates are in close agreement with respect to the maximum values of circulation achieved and the rate of loss of circulation from maximum to zero. However, unlike the experimental results the circulation measured in the model *Drosophila* wing falls to zero at  $\hat{r}=0.85$  as compared to the theoretical circulation that becomes zero only at  $\hat{r}=1$ . Most likely, this discrepancy arises due to exclusion of wing tip losses from the theoretical model.

#### A tentative incorporation of Prandtl's tip loss approximation

For any finite flapping or translating airfoil, it is necessary to take into account the effect of tip vortices when addressing the overall structure of the flow fields. Physically, ignoring

these tip losses amounts to assuming that the aerodynamic effect of wing tip is small compared to the chordwise circulation and that each section of the wing continues to generate lift all along the span. As first pointed out by Prandtl (Prandtl and Tietjens, 1957) this assumption may not be valid at points closer to the tip of a finite wing, where a tip vortex enhances leakage of the fluid around the airfoil tip thus significantly reducing the ability of that region to generate any lift. In the framework described above, the effect of tip vortices is not considered explicitly, but is implicitly incorporated through the measured lift coefficients, which include the effect of tip vorticity on the finite wings and through the semi-elliptic distribution resulting from the loss of lift at wing tips.

Many recent experimental results clearly document the effect of tip vortices on the overall flow field in flapping wings. Willmott et al. (1997) showed there were significant tip vortices during both upstroke and downstroke on the wings of moths actively flapping in a smoke rake, confirming the presence of bound circulation and force generation on both strokes. In CFD simulations on 'virtual' hawk moths, Liu et al. (1998; Liu and Kawachi, 1998) confirmed this flow around the tip. While visualizing flow around flapping model wings, Birch and Dickinson (2001) noted a distinct spanwise change in the downwash velocity likely influencing the sectional angles of attack.

In an appendix to a paper by Betz (1919), Prandtl suggested a formula to calculate the loss in lift generating ability due to the leakage around wing tips, expressed in terms of a reduction in the effective blade length or the actuator disk area (Seddon,

1990). This formula and its subsequent modifications by other researchers (for a review, see Johnson, 1980) do not have a rigorous theoretical basis but are known to work well over a large data set on rotors. According to his formula, the ratio ( $k$ ) of the effective wing span generating lift over the total wing span is given by:

$$k = 1 - \left[ \frac{1.386}{N} \left( \frac{v_i}{u_\infty} \right) \right], \quad (41)$$

where  $N$  is the number of blades of a propeller system. Application of this formula to the insect flight case must be made with some caution. First, for  $0 < \hat{x} < 1$  the determination of the integral in  $s_i(\hat{x})$  is complicated due to singularity at the point  $\hat{r} = \hat{x}$  along the span. For the specific case  $s_i(0)$ , we can approximately calculate the effect of tip losses by assuming a uniform inflow across the wing blade and setting

$$\frac{v_i(R)}{u_\infty(R)} = \frac{v_i(0)}{\bar{u}_\infty}, \quad (42)$$

where

$$\bar{u}_\infty = \frac{2\Phi n R \int_0^1 \hat{r} d\hat{r}}{\int_0^1 d\hat{r}} = \Phi n R. \quad (43)$$

Substituting Eqn 25 and 44 into Eqn 43 gives:

$$\frac{v_i(0)}{u_\infty} = \frac{\bar{C}_L \bar{c} B_{fly}}{2\pi R} s_i(0) \quad (44)$$

and

$$k = 1 - \frac{1.386}{N} \left( \frac{\bar{C}_L \bar{c} B_{fly}}{2\pi R} s_i(0) \right). \quad (45)$$

Second, because the formula was developed for a rotor with variable number of blades, it is not immediately clear if insect wings should be considered as a two-blade or a single-blade system. For a single (up or down) stroke, the net angular excursion of the two wing-system is similar to that of a single-blade rotor in full revolution i.e.  $N=1$ . For a complete wing cycle, however the two-wing system behaves like a two-blade rotor because each wing goes through an angular excursion of (approximately)  $2\pi$ , i.e.  $N=2$ .

For  $N=1$ , using representative values of  $\bar{C}_L=1.8$ ,  $\bar{c}=0.7$  mm,  $R=2.5$  mm, and  $B_{fly}s_i(0)=0.79$  (where  $B_{fly}=3.2$ ), the ratio of the effective wing span to actual wing span  $k$  is about 0.72. For  $N=2$ , the value  $k$  is approximately 0.86. Thus, depending on the value of  $N$  chosen, the calculations estimate that about 14–28% of the wing span from the wing tip produces no lift, as compared to the experimental values of about 15%. Although Prandtl's basic approach could enable us to

approximate tip losses in flapping insect wings, it is important to view the above result with some caution because the assumption of uniform inflow may not be valid in most cases.

#### Induced air flow due to flapping wings in the near-field

In the few cases where flow was visualized and quantified around an insect body, the insects were placed within wind tunnels in the presence of an ambient flow typically equal to or higher than the induced axial velocity to ensure that the seeding particles streamed along the insect body (Dickinson and Gotz, 1996; Bomphrey et al., 2005). The ambient flow in Dickinson and Gotz (1996) is  $20 \text{ cm s}^{-1}$  as compared to the axial inflow estimate of  $14.8 \text{ cm s}^{-1}$ . In Bomphrey et al. (2005), the ambient flow is  $3.5 \text{ m s}^{-1}$  and  $1.2 \text{ m s}^{-1}$  as compared to the estimated axial inflow range of  $0\text{--}0.35 \text{ m s}^{-1}$ . Hence, I was unable to use these studies to test the induced flow model described above.

#### Case study: *Manduca sexta*

The predictions of this model for axial inflow were tested using hot wire anemometry to measure the airflow between the antennae of a flapping hawk moth, *Manduca sexta* (see accompanying article by Sane and Jacobson, 2006). For a *Manduca* wing, the form of  $\hat{c}(\hat{r})$  can be approximated by the Eqn 19 using:

$$\hat{c}(\hat{r}) = \hat{r}^{0.125} (1-\hat{r})^{0.5}. \quad (46)$$

When the wing rotates steadily around an axis, the post-downwash lift coefficients vary between 0 to 1.25 (Usherwood and Ellington, 2002). Using the representative values of  $\Phi=2\pi/3$  radians,  $n=25$  Hz,  $\bar{c}=0.02$  m.,  $B_{moth}s_i=0.8673$  (where  $B_{moth}=1.8$ ), the range of mean axial velocity calculated by Eqn 27 falls between 0 and  $0.35 \text{ m s}^{-1}$ . This range matches rather well with the observed range for the induced axial inflow in flapping *Manduca sexta* from the anemometric measurements (fig. 5 in the accompanying article, Sane and Jacobson, 2006).

Thus, the theory presented here is capable of approximately predicting the mean induced flow speeds due to flapping wings in both the near- and far-field. It shows that this flow is directly proportional to the stroke frequency and amplitude, provided the wing shape and angle of attack remain constant or change only slowly. These equations may be useful to a broad variety of researchers studying such diverse topics as odor tracking behavior, convective heat loss or gas exchange in flying insects, all of which may be influenced by the structure of flow over their bodies.

#### List of symbols

$A$	area of actuator disk
$\mathcal{R}$	aspect ratio
$B_i$	chord rescale ratio
$\bar{c}$	mean chord length
$c(r)$	chord length as a function of radial position
$\hat{c}(\hat{r})$	non-dimensional chord length

$C_L$	lift coefficient
$\bar{C}_L$	mean coefficient of lift (average of sections from base to tip of a finite wing)
$C_L(\hat{r})$	spanwise coefficient of lift
$\dot{\phi}$	angular velocity of the wing
$F_L$	lift
$g$	gravitational acceleration
$k$	ratio of the effective wing span to actual wing span
$K_0$	proportionality constant
$m$	mass of insect
$n$	wing beat frequency
$P$	mean pressure above actuator disk
$p, q$	powers of the Beta function describing wing shape
$P_0$	ambient pressure
$\hat{r}$	non-dimensional radial position
$r$	position along the wing measured from base to tip
$R$	wing length
$s_i(0)$	a shape parameter at $\hat{x}=0$
$s_i(\hat{x})$	a shape parameter as a function of $\hat{x}$
$u_\infty(r)$	wing velocity
$v_{\text{axial}}$	axial flow velocity
$\bar{v}_{\text{far}}$	mean far field induced flow
$v_i$	induced velocity
$v_i(\hat{x})$	induced velocity at $\hat{x}$
$\bar{v}_i$	mean near-field induced flow
$x, \hat{x}$	distance from wing base of an arbitrary point on or near the moving wing
$\Phi$	stroke amplitude
$\Gamma(r)$	circulation as a function of radial position
$\Gamma_0$	spanwise circulatory component of the series expansion of circulation
$\Gamma_2, \Gamma_4, \dots$	second, fourth etc. derivatives of the circulation with respect to $\hat{r}$
$\Gamma_{2D}(r)$	spanwise circulation of a wing section
$\Gamma_f(\hat{r})$	spanwise circulation of a finite wing
$\alpha$	morphological angle of attack
$\alpha'(\hat{x})$	spanwise effective angle of attack
$\rho$	air density

I am grateful to Tom Daniel, Michael Dickinson and Ty Hedrick and Sudip Seal for providing useful comments. This work was supported by an NSF Inter-Disciplinary Informatics grant to Sanjay P. Sane and an ONR-MURI grant to Tom Daniel.

### References

**Betz, A. and Prandtl, L.** (1919). Schraubenpropeller mit geringstem Energieverlust. *Nachr. Ges. Wiss. Göttingen* **1919**, 193-213.

**Birch, J. and Dickinson, M. H.** (2001). Spanwise flow and the attachment of the leading-edge vortex. *Nature* **412**, 729-733.

**Birch, J. M. and Dickinson, M. H.** (2003). The influence of wing-wake interactions on the production of aerodynamic forces in flapping flight. *J. Exp. Biol.* **206**, 2257-2272.

**Birch, J. M., Dickson, W. B. and Dickinson, M. H.** (2004). Force production and flow structure of the leading edge vortex on flapping wings at high and low Reynolds numbers. *J. Exp. Biol.* **207**, 1063-1072.

**Bomphrey, R. J., Lawson, N. J., Harding, N. J., Taylor, G. K. and Thomas,**

**A. L. R.** (2005). The aerodynamics of *Manduca sexta*: digital particle image velocimetry analysis of the leading-edge vortex. *J. Exp. Biol.* **208**, 1079-1094.

**Conlisk, A. T.** (1997). Modern helicopter aerodynamics. *Annu. Rev. Fluid Mech.* **29**, 515-567.

**Dickinson, M. H.** (1994). The effects of wing rotation on unsteady aerodynamic performance at low Reynolds numbers. *J. Exp. Biol.* **192**, 179-206.

**Dickinson, M. H. and Gotz, K. G.** (1996). The wake dynamics and flight forces of the fruit fly *Drosophila melanogaster*. *J. Exp. Biol.* **199**, 2085-2104.

**Dickinson, M. H., Lehmann, F. O. and Sane, S. P.** (1999). Wing rotation and the aerodynamic basis of insect flight. *Science* **284**, 1954-1960.

**Dickson, W. B. and Dickinson, M. H.** (2004). The effect of advance ratio on the aerodynamics of revolving wings. *J. Exp. Biol.* **207**, 4269-4281.

**Ellington, C. P.** (1974). Non-steady-state aerodynamics of the flight of *Encarsia formosa*. In *Swimming and Flying in Nature*, Vol. 2 (ed. C. J. Brokaw, C. Brennen and T. Y.-T. Wu), pp. 783-796. New York, London: Plenum Press.

**Ellington, C. P.** (1984a). The aerodynamics of hovering insect flight. II. Morphological parameters. *Phil. Trans. R. Soc. Lond. B* **305**, 17-40.

**Ellington, C. P.** (1984b). The aerodynamics of hovering insect flight. III. Kinematics. *Phil. Trans. R. Soc. Lond. B* **305**, 41-114.

**Ellington, C. P.** (1984c). The aerodynamics of hovering insect flight. V. A vortex theory. *Phil. Trans. R. Soc. Lond. B* **305**, 115-144.

**Ellington, C. P., vandenBerg, C., Willmott, A. P. and Thomas, A. L. R.** (1996). Leading-edge vortices in insect flight. *Nature* **384**, 626-630.

**Johnson, W.** (1980). *Helicopter Theory*. Princeton: Princeton University Press.

**Jones, R. T.** (1990). *Wing Theory*. Princeton: Princeton University Press.

**Kuethe, A. M. and Chow, C.-Y.** (1986). *Foundations of Aerodynamics*. New York: John Wiley and Sons.

**Lehmann, F. O., Sane, S. P. and Dickinson, M.** (2005). The aerodynamic effects of wing-wing interaction in flapping insect wings. *J. Exp. Biol.* **208**, 3075-3092.

**Leishman, J. G.** (2000). *Principles of Helicopter Aerodynamics*. Cambridge: Cambridge University Press.

**Liu, H. and Kawachi, K.** (1998). A numerical study of insect flight. *J. Comput. Phys.* **146**, 124-156.

**Liu, H., Ellington, C. P., Kawachi, K., Van den Berg, C. and Willmott, A. P.** (1998). A computational fluid dynamic study of hawkmoth hovering. *J. Exp. Biol.* **201**, 461-477.

**Maybury, W. J. and Lehmann, F. O.** (2004). The fluid dynamics of flight control by kinematic phase lag variation between two robotic insect wings. *J. Exp. Biol.* **207**, 4707-4726.

**Miller, L. A. and Peskin, C. S.** (2005). A computational fluid dynamics of 'clap and fling' in the smallest insects. *J. Exp. Biol.* **208**, 195-212.

**Milne-Thomson, L. M.** (1973). *Theoretical Aerodynamics*. New York: Dover Publications.

**Minotti, F.** (2002). Unsteady two-dimensional theory of a flapping wing. *Phys. Rev. E* **66**, 051907.

**Prandtl, L. and Tietjens, O. K. G.** (1957). *Applied Hydro- and Aeromechanics: Based on Lectures of L. Prandtl*. New York: Dover Publications.

**Ramamurti, R. and Sandberg, W. C.** (2002). A three-dimensional computational study of the aerodynamic mechanisms of insect flight. *J. Exp. Biol.* **205**, 1507-1518.

**Rayner, J. M. V.** (1979). Vortex theory of animal flight I. vortex wake of a hovering animal. *J. Fluid Mech.* **91**, 697-730.

**Sane, S. P.** (2003). The aerodynamics of insect flight. *J. Exp. Biol.* **206**, 4191-4208.

**Sane, S. P. and Dickinson, M. H.** (2001). The control of flight force by a flapping wing: lift and drag production. *J. Exp. Biol.* **204**, 2607-2626.

**Sane, S. P. and Dickinson, M. H.** (2002). The aerodynamic effects of wing rotation and a revised quasi-steady model of flapping flight. *J. Exp. Biol.* **205**, 1087-1096.

**Sane, S. P. and Jacobson, N. P.** (2006). Induced airflow in flying insects. II. Measurement of induced flow. *J. Exp. Biol.* **209**, 43-56.

**Seddon, J.** (1990). *Basic Helicopter Aerodynamics*. Washington DC: American Institute of Aeronautics.

**Srygley, R. B. and Thomas, A. L. R.** (2002). Unconventional lift-generating mechanisms in free-flying butterflies. *Nature* **420**, 660-664.

- Sun, M. and Tang, H.** (2002). Unsteady aerodynamic force generation by a model fruit fly wing in flapping motion. *J. Exp. Biol.* **205**, 55-70.
- Usherwood, J. R. and Ellington, C. P.** (2002). The aerodynamics of revolving wings. I. model hawkmoth wings. *J. Exp. Biol.* **205**, 1547-1564.
- VandenBerg, C. and Ellington, C. P.** (1997a). The three-dimensional leading-edge vortex of a 'hovering' model hawkmoth. *Phil. Trans. R. Soc. Lond. B* **352**, 329-340.
- VandenBerg, C. and Ellington, C. P.** (1997b). The vortex wake of a 'hovering' model hawkmoth. *Phil. Trans. R. Soc. Lond. B* **352**, 317-328.
- Wang, Z. J.** (2000). Two dimensional mechanism for insect hovering. *Phys. Rev. Lett.* **85**, 2216-2219.
- Wang, Z. J.** (2005). Dissecting insect flight. *Annu. Rev. Fluid Mech.* **37**, 183-210.
- Wang, Z. J., Birch, J. M. and Dickinson, M. H.** (2004). Unsteady forces and flows in low Reynolds number hovering flight: two-dimensional computations vs robotic wing experiments. *J. Exp. Biol.* **207**, 449-460.
- Willmott, A. P., Ellington, C. P. and Thomas, A. L. R.** (1997). Flow visualization and unsteady aerodynamics in the flight of the hawkmoth, *Manduca sexta*. *Phil. Trans. R. Soc. Lond. B* **352**, 303-316.
- Zbikowski, R.** (2002). On aerodynamic modelling of an insect-like flapping wing in hover for micro air vehicles. *Phil. Trans. R. Soc. Lond. B* **360**, 273-290.